Settling Velocities of Fractal Aggregates

CLIFFORD P. JOHNSON, XIAOYAN LI, AND BRUCE E. LOGAN*

Department of Chemical and Environmental Engineering, University of Arizona, Tucson, Arizona 85721

Aggregates generated in water and wastewater treatment systems and those found in natural systems are fractal and therefore have different scaling properties than assumed in settling velocity calculations using Stokes' law. In order to demonstrate that settling velocity models based on impermeable spheres do not accurately relate aggregate size, porosity and settling velocity for highly porous fractal aggregates, we generated fractal aggregates by coagulation of latex microspheres in paddle mixers and analyzed each aggregate individually for its size, porosity, and settling velocity. Settling velocities of these aggregates were on average 4−8.3 times higher than those predicted using either an impermeable sphere model (Stokes' law) or a permeable sphere model that specified aggregate permeability for a homogeneous distribution of particles within an aggregate. Fractal dimensions (D) derived from size−porosity relationships for the three batches of aggregates were 1.78 ± 0.10, 2.19 ± 0.12 and 2.25 ± 0.10. These fractal dimensions were used to predict power law relationships between aggregate size and settling velocity based on Stokes' law. When it was assumed that the the drag coefficient, C_D, was constant and fixed at its value of $C_D = 24/Re$ for the creeping flow region ($Re \ll 1$), predicted slopes of size and settling velocity were in agreement with only the data sets where $D > 2$. As a result, when $D < 2$, aggregate porosities will be overestimated and fractal dimensions will be calculated incorrectly from settling velocity data and Stokes' law.

Introduction

Particle transport by gravitational sedimentation is important in nearly all water and wastewater treatment processes. Particles settle out in clarifiers following chemical addition and flocculation in conventional water treatment process trains, and microbial aggregates formed in activated sludge aeration tanks and other bioreactors are also removed by settling in clarifiers. Substantial research indicates that these aggregates have fractal geometries (*1*, *2*). The equations used to model particle settling in coagulation (*3*) and sedimentation tanks (*4*) and filtration columns (*5*, *6*), however, are usually based on the description of the particles as spheres. The settling velocities of aggregates obtained from natural systems (*7*) or those produced in the laboratory (*8*, *9*) have also been analyzed by assuming that the aggregate has settling properties similar or identical to those of impermeable spheres. Such assumptions have made it difficult to reconcile observed and predicted settling velocities of these aggregates.

The settling velocities of isolated impermeable solid particles are well predicted using widely available equations and correlations (*10*). Settling velocities of highly porous aggregates have also been experimentally measured, although aggregates in these studies were not shown to be fractal (*11*, *12*). There have been efforts to calculate settling velocities of aggregates as permeable porous spheres (*13*, *14*) and as permeable fractal aggregates (*15*), but the equations used in all these investigations have been based on permeability correlations that assume a homogeneous distribution of particles within the aggregate. Accurate equations for relating settling velocity to other aggregate properties such as porosity, density, and mass are important since these other properties are often calculated from settling velocity data by assuming that Stokes' law is valid (*8*, *9*, *16*). The use of inaccurate settling equations could naturally lead to significant errors in these reported aggregate properties.

In this study, we present data on the settling velocities of a population of fractal aggregates varying in size from 100 to 1000 μm. These aggregates were generated from dyed latex microspheres in standard paddle mixers and analyzed independently for size, settling velocity, density and fractal dimension. Our results indicate that fractal aggregates settle on average 4−8.3 times faster (range 2−20 times) than calculated using Stokes' law even after inclusion of their nonconstant aggregate density. We attribute this difference to substantially different drag relationships for fractal rather than equivalent sized spherical particles. Our findings have important implications for the interpretation of aggregate densities and fractal dimensions determined in previous studies from settling velocity data.

Methods

The settling velocity of an impermeable spherical aggregate can be predicted from Stokes' law. Most aggregates however are not spherical, and it is thought that they are permeable. This has led to the proposal of several different scaling relationships between aggregate size and settling velocity for fractal aggregates. In order to show how different assumptions of either Euclidean or fractal properties affect predictions of settling velocity as a function of aggregate size, we review Stokes' law below. This derivation will allow us to show how fractal dimensions have been deduced from size-settling velocity relationships.

Theoretical Section. *Impermeable Spherical Aggregates.* The settling velocity of a spherical impermeable aggregate is calculated from a force balance, producing Stokes' law (*10*). There are three forces, gravity (F_g), buoyant (F_b), and drag (F_d), acting upon an aggregate, which balance according to

* Corresponding author telephone: 520-621-4316; fax: 520-621-6048; e-mail address: logan@bigdog.engr.arizona.edu.

S0013-936X(95)00604-3 CCC: $12.00

$$F_g - F_b = F_d \quad (1)$$

Since $F_g = \rho_a V_a g$, where ρ_a is the aggregate density, g is the gravitational constant, and $F_b = \rho_l V_a g$, where ρ_l is the suspending liquid density, the sum of the gravity and buoyant forces can be replaced in this relationship as

$$V_a(\rho_a - \rho_l)g = F_d \quad (2)$$

If all particles composing the aggregate have the same density ρ_p, the density difference in eq 2 can be equivalently written using the identities

$$(\rho_a - \rho_l) = (1 - p)(\rho_p - \rho_l) = (1 - p)\,\Delta\rho \quad (3)$$

where p is the aggregate porosity and $\Delta\rho$ is the difference between the particle and fluid densities. The drag force exerted on an object is expressed as a function of the fluid density and the object's velocity (U), projected area (A), and an empirical drag coefficient (C_d). Using the common expression that $F_d = \rho U^2 A C_d/2$ (*10*), eq 2 can be written as

$$V_a(1 - p)\Delta\rho g = \rho_l U^2 A C_d/2 \quad (4)$$

At this point in the derivation we must use geometrical relationships to simplify eq 4. For spheres

$$V_a = \frac{\pi}{6} d^3 \quad (5)$$

$$A = \frac{\pi}{4} d^2 \quad (6)$$

$$C_d = \frac{24}{Re} \qquad (Re \ll 1) \quad (7)$$

where the Reynolds number $Re = Ud/\nu$, d is the aggregate diameter, and ν is the fluid kinematic viscosity (*17*). Combining eqs 4−7, produces Stokes' law:

$$U = \frac{g\Delta\rho(1 - p)}{18\nu\rho_l} d^2 \quad (8)$$

For an aggregate made up of N particles each of mass m_o and volume v_o, the porosity can be derived in terms of

$$(1 - p) = \frac{N v_o}{V_a} \quad (9)$$

where the percent solids in an aggregate is calculated as $100(1 - p)$. Substituting eq 9 into eq 8 and assuming aggregate volume as defined in eq 5 produces

$$U = \frac{g\Delta\rho N v_o}{3\pi\nu\rho_l d} \quad (10)$$

The predicted settling velocity in eq 10 can be compared to the actual settling velocity, U_{act}, using the dimensionless number, Γ, defined as

$$\Gamma = \frac{U_{act}}{U} \quad (11)$$

Calculation of a Fractal Dimension from Scaling Relationships. It is commonly observed that for aggregates U is not proportional to d^2, but to d^c where c is some value less than 2 (*7*, *8*, *16*). The reason for this difference from Stokes' law was attributed by Li and Ganczarczyk (*1*) only to the assumption that the aggregate porosity was not constant. The nonlinear relationship between aggregate size and porosity is a consequence of the fractal geometry of aggregates. It is well known for colloidal aggregates that the mass of the aggregate scales with its size, l, according (18) to

$$m \sim l^D \quad (12)$$

where D is a three dimensional fractal dimension. Since the mass of an aggregate is related to the number of particles in the aggregate by $m = N m_o$, it follows that

$$N \sim l^D \quad (13)$$

Using eqs 5, 9, and 13, we can therefore derive the fractal scaling relationship

$$(1 - p) \sim l^{D-3} \quad (14)$$

Assuming that the length scales l and d are the same, the following scaling relationship can be derived from eqs 8 and 14 between settling velocity and aggregate size:

$$U \sim l^{D-1} \quad (15)$$

Thus it was proposed (*1*) that the fractal dimension D could be derived from the slope of a log−log plot of settling velocity and aggregate size.

It has been suggested by others (*2*, *19*) that the geometrical and empirical relationships (eqs 6 and 7) assumed to derive eq 12 might not be valid for all fractal inorganic and organic aggregates. Logan and Wilkinson (*2*) proposed that the area-length equation also be cast in terms of a fractal dimension as

$$A \sim l^{D_2} \quad (16)$$

where D_2 is a two-dimensional fractal dimension. When $D < 2$, a colloidal aggregate viewed in two dimensions is transparent since all particles are visible, and $D_2 = D$. However, when $D \geq 2$, then $D_2 = 2$ (*18*). When eq 16 is used instead of eq 6, settling velocity scales according to

$$U \sim l^{D-D_2+1} \quad (17)$$

Jiang and Logan (*19*) proposed a settling velocity relationship that could be used when Reynolds numbers were not in the creeping flow region. They used drag coefficients developed for spheres only because no such correlations were available for fractal aggregates. They fit the empirical drag correlation (*17*) with the power law relationship

$$C_d = aRe^{-b} \quad (18)$$

where for $Re \ll 1$, $a = 24$ and $b = 1$ and for $0.1 < Re < 10$, $a = 29.03$ and $b = 0.871$. Incorporating eqs 16 and 18 into the derivation of a scaling relationship for settling velocity produced

$$U \sim l^{(D-D_2+b)/(2-b)} \quad (19)$$

These relationships are summarized in Table 1 for different ranges of Reynolds numbers and fractal dimensions.

Homogeneous Permeable Spherical Aggregates. Flow through the interior of an aggregate can increase the settling velocity of an aggregate compared to otherwise identical

TABLE 1

Scaling Relationships Used To Calculate Fractal Dimensions from Settling Velocity Data Based on Different Assumptions of Aggregate Properties

general expression	conditions	if $D < 2$	if $D \geq 2$	ref
$U \sim l^{D-1}$	$Re \ll 1$	$U \sim l^{D-1}$	$U \sim l^{D-1}$	1
$U \sim l^{D-D_2+1}$	$Re \ll 1$	$U \sim l$	$U \sim l^{D-1}$	2
$U \sim l^{(D-D_2+b)/(2-b)}$	$Re \ll 1$ $b = 1$	$U \sim l$	$U \sim l^{D-1}$	19
$U \sim l^{(D-D_2+b)/(2-b)}$	$0.1 < Re < 10$ $b = 0.871$	$U \sim l^{0.77}$	$U \sim l^{0.89(D-1)}$	19

but impermeable particles. The settling velocity of a permeable aggregate was presented by Masumoto and Suganuma (*11*) as

$$U_{\text{perm}} = U\left[\frac{\xi}{\xi - \tanh(\xi)} + \frac{3}{2\xi^2}\right] \qquad (20)$$

where the dimensionless variable $\xi = d/(2\kappa^{1/2})$ relates aggregate size to permeability of the porous media. The main difficulty in applying eq 20 to fractal aggregates is that permeability functions used in previous investigations (*14*, *15*) have been developed for homogeneous media. Logan and Hunt (*14*) used the Davies correlation (*12*)

$$\frac{1}{\kappa} = \frac{16}{a_{\text{cyl}}^2}(1-p)^{1.5}[1 + 56(1-p)^3] \qquad (21)$$

where κ is the aggregate permeability and a_{cyl} is the radius of a long filament assumed to form the aggregate. Even after accounting for aggregate size−porosity relationships, Logan and Hunt calculated that the power in a size-settling velocity relationship was only increased slightly from $U \sim d^{0.4}$ to $U_{\text{perm}} \sim d^{0.44}$ as a result of aggregate permeability. Others have predicted similarly small changes in settling velocities due to aggregate permeability (*20*). The main reason for deviations from Stokes' law in experimental observations (*8*, *9*) is thought to be a result of nonlinear relationships between aggregate size and porosity (*14*).

Experimental Section. *Generation of Fractal Aggregates.* The aggregates used in settling experiments were generated from latex microspheres (Polysciences Inc.) 2.6 μm (red beads, experiments 1 and 2) or 0.87 μm (yellow-green beads, experiment 3) in diameter with a density of 1.05 g cm^{-3} specified by the manufacturer and verified by us as 1.050 ± 0.003 g cm^{-3} using a Percoll density gradient. Microspheres (2.5% suspension by weight) were coagulated in NaCl solutions (average density of 2.5%) in a paddle mixer (Phipps and Bird Model 7790−400) at 10 rpm using 1000-mL round beakers filled to 500 mL and standard flat paddles (19.2 cm^2 surface area). A shear rate of 5 s^{-1} was estimated from Lai et al. (*21*) for these conditions. In experiment 1, aggregates formed within 24 h. Although the same salt concentrations were used in all three experiments, aggregates generated during experiments 2 and 3 took longer to form (∼48−72 h). This likely resulted in aggregate breakup and re-aggregation being more important in forming aggregates in experiments 2 and 3 than these processes were in experiment 1.

Settling Column. Settling experiments were performed in 20 cm high acrylic settling columns 3.15 cm in diameter mounted on sliding base plates (Figure 1). The diameter of the column was selected to minimize wall effects on settling aggregates based on calculations using the Faxen friction factor (*22*). For spheres 50−500 μm in diameter, the drag of the cylinder wall was calculated to increase drag by less than 3.2%. Settling velocities were measured at a depth of 15−20 cm below the release point based on experiments indicating that aggregate terminal velocities were reached within 15 cm. The top of the column was sealed with a rubber stopper containing a small tube to allow introduction of aggregates. Sealing the top of the column was necessary to avoid convective currents in the column during settling experiments.

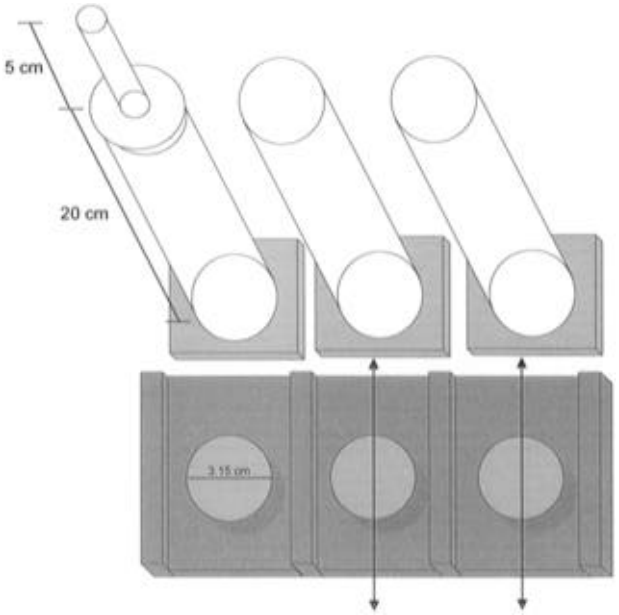

FIGURE 1. Settling columns used in experiments.

The columns were designed with retrieval wells to allow the recovery of aggregates after a settling experiment. The flat bottom of the column base was sealed to the well base using silicon vacuum grease. After a settling experiment, the column base was pushed to the side and the column was removed, leaving the aggregate in the bottom well (depth = 0.8 cm) for subsequent analysis.

Settling Experiments. Three separate batches of aggregates generated in the paddle mixers were used in settling experiments. Water used in the paddle mixer was identical to that in the settling column. To ensure that the salinity of the water in the aggregates was exactly the same as that in the settling column (i.e., to ensure that salinity of the water in the covered beakers in the paddle mixer did not change by evaporation), individual aggregates were transferred through three separate beakers in series (over a time period of 20 min), each containing water identical to that placed in the settling column. Each aggregate was transferred using a P-1000 pipetteman (Rainin) with the 1-mL pipet tip cut midway to minimize breakup of the aggregate. The aggregate was then placed into the top of the settling column, and the settling velocity at a point 15−20 cm from the top of the column was recorded using a Sony CCD camera with a macrolens connected to a four-head VCR (JVC Corp.). The column was illuminated using a fiber optic light source. The settling velocity was measured using a stopwatch as the time for the aggregate to transverse the field of vision (4.0 ± 0.5 cm) to within 0.25 s.

The accuracy of the settling column was tested in settling experiments using individual polystyrene beads (density of 1.05 g cm^{-3}) ranging from 400 to 500 μm in diameter

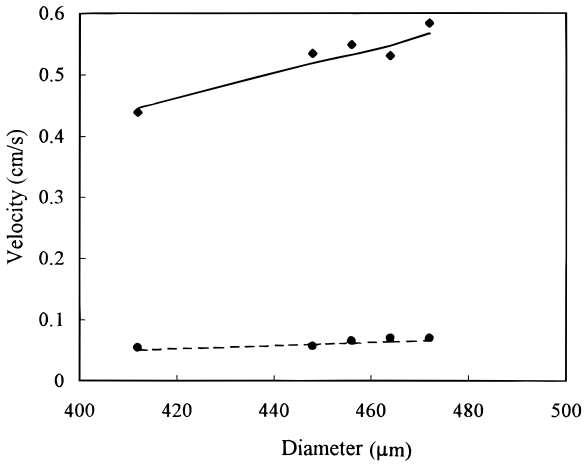

FIGURE 2. Comparison of observed (points) settling velocities versus those predicted using Stokes' law (lines) for solid spheres ($\rho = 1.05$ g cm^{-3}) in ultrapure water ($\rho_l = 0.998$ g cm^{-3}; ♦ and solid line) and a NaCl solution ($\rho_l = 1.0446$ g cm^{-3}; ● and dashed line).

(Figure 2). Settling velocities of these beads in ultrapure water (Milli-Q) of density 0.998 g cm^{-3} were within 3.5% of values calculated using Stokes' law (eq 8). In a NaCl solution ($\rho_l = 1.0446$ g cm^{-3}), measured settling velocities were all <10% of predicted values (average 7.2%).

Aggregate Properties. The cross sectional areas of aggregates were measured by placing the column base containing an aggregate from a settling experiment on a microscope (Olympus BH-2) stand for aggregate sizing using an image analysis system (Galai Scan Array) at 100×. Aggregates were viewed under bright field (red beads) or blue light (yellow-green fluorescent beads). Aggregate size was calculated as an equivalent diameter using $d = (4A/\pi)^{1/2}$.

After sizing, individual aggregates were collected from the column well using a pipet tip, transferred into a container containing ultrapure water, shaken, sonicated for 1 h, and filtered onto a plain (red beads) or black (yellow-green beads) 0.4 μm pore diameter polycarbonate filter (25 mm diameter, Poretics Corp.). Filters were mounted onto glass slides, and 20−50 fields were counted under white or blue light at 1000×. The total number of beads was obtained by multiplying the average number of beads per field by the ratio of the total and view areas.

Aggregate encased volume and porosity were calculated using eqs 5 and 9. The average fractal dimension for each of the three batches of aggregates was calculated using eq 13, and the Stokes' settling velocity was predicted using eq 10. The velocities of permeable aggregates were predicted using Stokes' law and eqs 20 and 21. Additional details of the experiments are given in ref 23.

Results

Fractal Dimensions. A total of 215 aggregates generated in three separate coagulation experiments were successfully captured during settling velocity experiments and analyzed. Aggregates that broke up during settling or any transfer step were discarded. Using eq 13, the fractal dimensions were calculated as 1.79 ± 0.10, 2.19 ± 0.12, and 2.25 ± 0.10 for the three different batches of aggregates (Figure 3). Different size−solid volume relationships were produced in experiments 2 and 3 even though the fractal dimensions were similar likely as a result of the different sizes of the

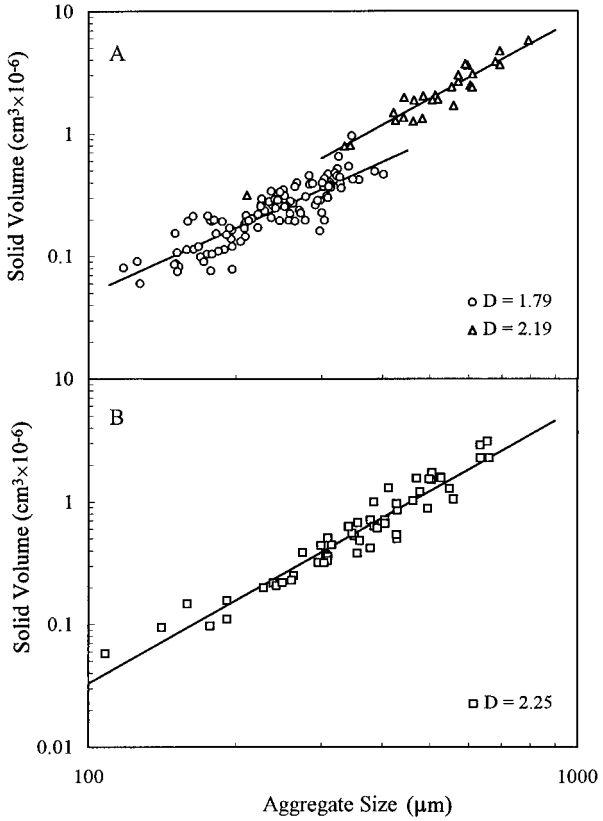

FIGURE 3. Fractal dimensions of three different batches of aggregates generated in a paddle mixer calculated from the slope of the regression lines (A) ○, experiment 1, $D = 1.79 \pm 0.10$ from solid line; △, experiment 2, $D = 2.19 \pm 0.12$ from dashed line; (B) □, experiment 3, $D = 2.25 \pm 0.10$ from solid line).

beads used to generate the aggregates (2.6 μm in experiments 1 and 2 and 0.87 μm in experiment 3).

Settling Velocities Compared to Impermeable Aggregates. The observed settling velocities of microsphere aggregates were consistently higher than those predicted from Stokes' Law for aggregates of identical size, mass and primary particle density (Figure 4). The dimensionless ratio of the observed to predicted velocities, Γ, ranged from 2 to 20 (Figure 5) with averages for experiments 1, 2, and 3 of $\Gamma = 8.3 \pm 4.0$ ($n = 110$), $\Gamma = 4.0 \pm 1.2$ ($n = 40$), and $\Gamma = 6.5 \pm 2.9$ ($n = 65$), respectively. This ratio did not appear to vary in proportion to the fractal dimension. All Γ data sets were significantly different from each other (Mann−Whitney Rank Sum Test) despite the overlap of the data. Levels of significance by experiment number were as follows: 1 and 2, 2 and 3, $p < 0.0001$; 1 and 3, $p < 0.0041$.

The predicted slopes of the settling velocity relationships were not significantly different than the observed slopes for the aggregates with $D \geq 2$ and when it was assumed that $Re \ll 1$ (Table 2, experiments 2 and 3). Since the fractal dimensions in experiments 2 and 3 were larger than 2, all creeping flow models predicted the slopes to be equal to $D - 1$. Based on the measured fractal dimensions, the predicted slopes were 1.19 and 1.25, while the observed slopes were 1.20 ± 0.11 and 1.33 ± 0.10. Two different slopes were calculated for the experiment with $D < 1$ (experiment 1), depending on whether D_2 was included (eq 15) in the calculation or not (eq 17). When D_2 was not included in the scaling relationship, the predicted slope of 0.79 was significantly less than the observed slope of 1.04 ± 0.10. Inclusion of D_2 resulted in a predicted slope of 1, in agreement with observations.

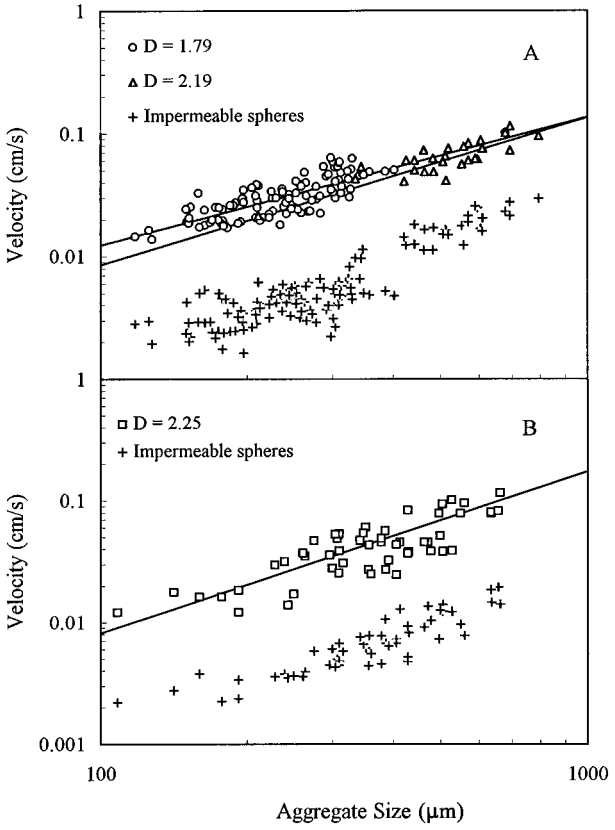

FIGURE 4. Settling velocities of aggregates predicted using Stokes' law (+) versus those observed in experiments: (A) ○, experiment 1, $D = 1.79$; △, experiment 2, $D = 2.19$; (B) □, experiment 3, $D = 2.25$. Slopes of the three lines are given in Table 2.

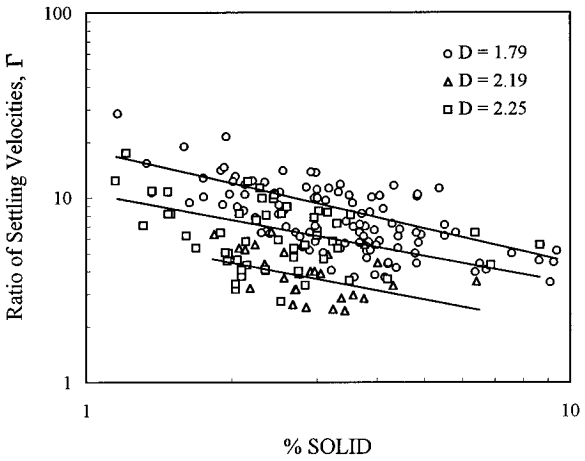

FIGURE 5. Dimensionless ratio (Γ) of observed and predicted aggregate settling velocities: (A) ○, experiment 1, $D = 1.79$; △, experiment 2, $D = 2.19$; (B) □, experiment 3, $D = 2.25$.

When drag coefficients were calculated based on larger *Re* numbers ($0.1 < Re < 10$) using $b = 0.871$ in eq 18, the observed slopes were always significantly larger than those predicted for spherical aggregates using independently measured parameters of D and D_2 in eq 19 (Table 2). The calculated slopes for $Re > 0.1$, however, included data for lower *Re* results ($Re < 0.1$) when $b = 1$. There was insufficient data to calculate a statistically significant slope when data with $Re < 0.1$ was excluded. We were therefore unable to test whether there was a significant change in the slopes for the different *Re* number ranges of $Re < 0.1$ and $Re > 0.1$.

TABLE 2

Comparison of Slopes from Settling Velocity Data with Those Predicted by Different Fractal Scaling Equations

relationship	conditions	expt 1 ($D < 2$)	expt 2 ($D \geq 2$)	expt 3 ($D \geq 2$)
data	$Re \ll 1$	1.04 ± 0.10	1.20 ± 0.11	1.33 ± 0.10
$U \sim l^{D-1}$	$Re \ll 1$	0.79	1.19	1.25
$U \sim l^{D-D2+1}$	$Re \ll 1$	1	1.19	1.25
$U \sim l^{(D-D_2+b)/(2-b)}$	$Re \ll 1$, $b = 1$	1	1.19	1.25
$U \sim l^{(D-D_2+b)/(2-b)}$	$0.1 < Re < 10$, $b = 0.871$	0.77	1.06	1.11

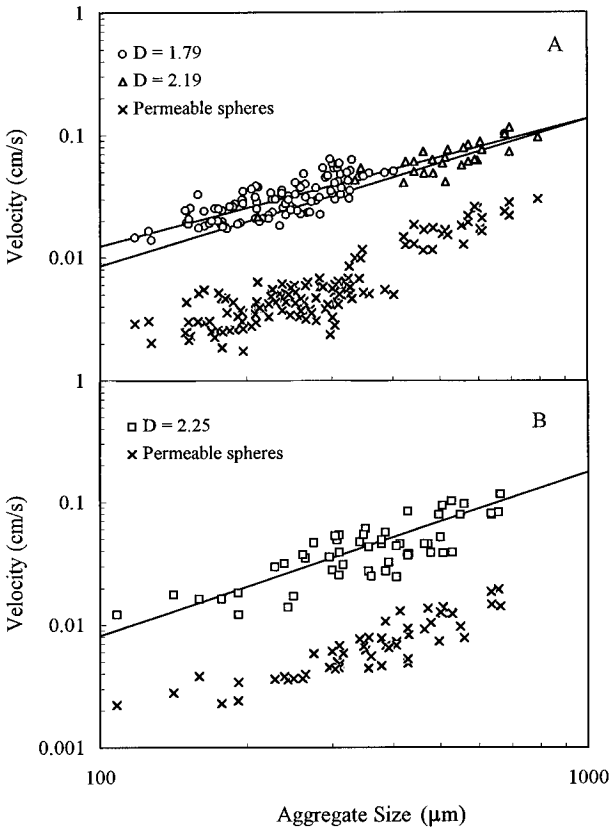

FIGURE 6. Settling velocities of aggregates predicted for permeable spherical aggregates (×) versus those observed in experiments: (A) ○, experiment 1, $D = 1.79$; △, experiment 2, $D = 2.19$; (B) □, experiment 3, $D = 2.25$. Slopes of the three lines are given in Table 2.

Settling Velocities Compared to Homogeneous Permeable Aggregates. Settling velocities predicted from permeability relationships developed for aggregates composed of particles distributed homogeneously throughout the aggregate were appreciably lower than observed velocities (Figure 6). The small increases in settling velocities predicted here are consistent with previous comparisons of impermeable and permeable aggregates (*14*, *15*). The observation that settling velocities of fractal aggregates are larger than predicted by permeable aggregate models means that permeability relationships derived for a homogeneous distribution of particles in a porous medium (such as eq 21) incorrectly describe the permeabilities of fractal porous media. The non-homogeneous distribution of particles in fractal aggregates results from the coagulation of small and more densely packed clusters into larger and overall less dense aggregates. The permeability of the

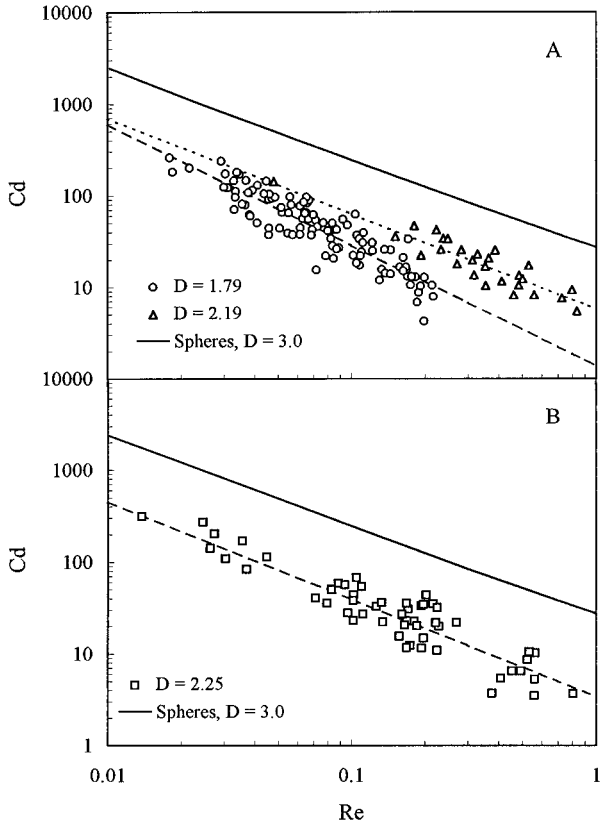

FIGURE 7. Drag coefficients calculated as a function of Reynolds number for a sphere (solid lines) versus experimental data: (A) ○, experiment 1, $D = 1.79$; △, experiment 2, $D = 2.19$; (B) □, experiment 3, $D = 2.25$. Slopes of the three regression lines (dashed lines) are given in Table 2.

TABLE 3

Empirical Drag Coefficient ($C_d = aRe^{-b}$) Constants for Different Fractal Dimensions

constant	experiment 1	experiment 2	experiment 3	impermeable sphere
D	1.79	2.19	2.25	3
a	0.14	0.75	0.52	24
b	1.31	1.04	1.05	1

macropores between clusters is likely to be much greater than the permeablity inside the smaller clusters, resulting in a non-uniform permeability within the porous aggregate.

Empirical Drag Coefficients of Fractal Aggregates. Based on these experimental results it was possible to calculate drag coefficients measured in the three experiments assuming the drag coefficient was adequately represented by the function $C_d = aRe^{-b}$, and assuming that all other geometrical factors were as specificed in Stokes' law. Re-deriving Stokes' law in terms of the drag coefficient and all directly measured values produced

$$C_d = \frac{2Nv_o\Delta\rho}{A\rho_l U^2} \tag{22}$$

The drag coefficients, derived from the plots in Figure 7, are summarized in Table 3. Since the slopes calculated from the size-settling velocity data compared well to predicted slopes for experiments 2 and 3, there were only small changes in the predicted constant b for different fractal dimensions. However, the much faster settling velocity of the fractal aggregates than spheres results in significantly lower values of the constant a when $D < 3$. Although this comparison suggests that the drag experienced by aggregates with fractal dimensions less than 2 is significantly different from those with $D > 2$, we have insufficient data at this time to include this observation into a method that incorporates the fractal dimension into a drag coefficient correlation.

Discussion

These experiments prove that fractal aggregates composed of inorganic microspheres can settle on average 4−8.3 times faster (range 2−20) than predicted by calculations for impermeable or permeable spheres of identical mass, cross sectional area, and primary particle density. These differences in settling velocities are likely a consequence of the heterogeneous distribution of primary particles in a fractal aggregate. As fractal aggregates increase in size, pores become larger, likely permitting greater quantities of flow through the aggregate interior than possible for permeable aggregates having a homogeneous distribution of particles within the aggregate. These large pores produce a smaller overall drag per total cross sectional area for the fractal aggregate than calculated for an impermeable or permeable spherical aggregate.

This finding that aggregates settle faster than predictions based on modified forms of Stokes' law is expected from previous comparisons of simulated settling velocities and experimentally measured properties of colloidal-sized fractal aggregates. Simulations of hydrodynamic friction, assumed to follow a Stokes−Einstein relationship, overestimated the friction of fractal objects such as macromolecules. Wiltzius (*24*) compared the size of aggregates measured by their radius of gyration, r_g, using static light scattering, to their hydrodynamic radius, r_h, calculated from quasielastic light-scattering experiments in terms of the ratio β, defined as

$$\beta = \frac{r_g}{r_h} \tag{23}$$

For aggregates in the size range of $500 \le r_h \le 7000$Å, Wilzius found that $\beta = 1.38$. This result was 2.4 times greater than simulations predicting $\beta = 0.57$.

Rogak and Flagan (*25*) computed the Stokes drag on self similar clusters of spheres by decomposing clusters of n monomers into smaller clusters which were replaced by hydrodynamically equivalent spheres. Their simulations predicted that β was a function of the fractal dimension and the number of monomers. For $D = 1.0$ (a single chain of particles) β ranged from 1 to 4 for $N = 10^2$−10^6. For larger fractal dimensions, increases in β were not as great. For $N = 10^2$−10^6, $\beta \approx 1.5$ for $D = 1.79$ and $\beta \approx 1.4$ for $D = 2.1$. Data from the three experiments reported here can be compared with Rojak and Flagan's results by using the relationship from their analysis that

$$r_g = r_f\left(\frac{D}{D+2}\right)^{1/2} \tag{24}$$

where r_f is the outer radius of the aggregate calculated from the size of the smallest circle that will just fully encompass the aggregate. The hydrodynamic radius is the aggregate diameter calculated in Stokes' law. Using $r_h = d/2$ and eq 10, r_h can be obtained from the measured

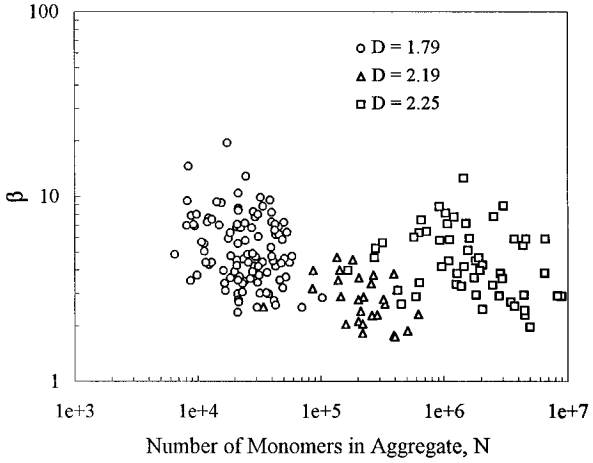

FIGURE 8. Dimensionless ratio (β) of the average and hydrodynamic radii as a function of the number of particles (N) in the aggregate: ○, experiment 1, $D = 1.79$; △, experiment 2, $D = 2.19$; □, experiment 3, $D = 2.25$.

parameters as

$$r_h = \frac{g\Delta\rho N v_o}{6\pi\nu\rho_l U} \tag{25}$$

Combining eqs 23−25, we have

$$\beta = \frac{6\pi\nu\rho_l U r_f D^{1/2}}{g\Delta\rho N v_o (D+2)^{1/2}} \tag{26}$$

Shown in Figure 8 is our settling data expressed in terms of β and the number of primary particles in the aggregate. The large differences in the number of beads in the two experiments with similar fractal dimensions result from the the generation of these aggregates from monomers of different sizes (2.6 μm diameter beads for $D = 2.19$ and 0.87 μm for $D = 2.25$). While there are clearly large variations in the data, calculated β's are larger by a factor of 2.7−6.4 than those predicted by Rogak and Flagan, indicating that their simulations of hydrodynamic friction of fractal aggregates overestimates the drag experienced by settling aggregates.

Since fractal aggregates experience less drag than predicted using Stokes' law, many previous studies have incorrectly calculated aggregate densities, porosities, primary particle densities or fractal dimensions from settling velocity data for aggregates with fractal dimensions less than 2. For example, Tambo and Watanabe (*16*) resolved observed settling velocities with those predicted using Stokes' law in eq 8 by assuming that the aggregate porosity could be described according to the function

$$(1-p) = ed^{-f} \tag{27}$$

A comparison of eq 27 with the fractal scaling relationship in eq 14 reveals that $f = 3 - D$. If we derive Stokes' law explicitly in terms of the drag relationship $C_d = aRe^{-b}$, assuming that $b = 1$, and replacing the power in eq 27 by the fractal relationship $D - 3$, we obtain

$$(1-p) = ed^{D-3} = \frac{3a\nu\rho_l U}{4g\Delta\rho d^2} \tag{28}$$

Equation 28 requires the drag experienced by a settling fractal aggregate to be identical to that of an impermeable sphere. Since the measured drag coefficients of fractal aggregates in this study were lower than those for impermeable spheres, reflected in lower values of a (Table 2), the aggregate porosity constant e would be overestimated by eq 28. If eq 28 were applied to data in our study, the aggregate solid fraction $(1 - p)$ would have been calculated to be 4−8.3 times greater than it actually was in order to account for the higher measured settling velocities than predicted using the impermeable sphere drag coefficient.

An additional problem with eq 28 is that it leads to the scaling relationship of $U \sim l^{D-1}$ (eq 15). Calculation of D using this approach is only valid when $D > 2$. If $D < 2$, D_2 must be included the scaling relationship (Table 2) since $D_2 \neq 2$ as it is for an impermeable sphere. If D_2 is not included, the magnitude of D will be overestimated. For example, D calculated for experiment 1 (where $D < 2$) using eq 15 produces $D = 2.04$ based on settling velocity data, but D is measured directly as $D = 1.79$ from size−porosity data.

Equation 28 can be modified to include D_2 by using eq 16 with a proportionality constant of h, to produce

$$U = \frac{eh}{3a}\frac{g\Delta\rho}{\nu\rho_l} d^{D-D_2+1} \tag{29}$$

While this equation will be correct for fractal geometry relationships, constants derived for eq 29 are not true constants. The constants will likely vary (as they have in this study) unless the aggregates all have the same fractal dimension and are developed from the same primary particles under identical conditions. The basis for this statement is that geometrical equations derived by Jiang and Logan (*19*) to describe aggregate morphology indicate that the constants e and h are functions of the fractal dimension. Results given in Table 3 show that a is a function of the fractal dimension as well. Thus, an empirical approach to the description of aggregate properties or settling velocity relationships should produce different constants for eq 25 under different conditions of aggregate growth. Surveys of fractal dimensions obtained for various types of aggregates produced under different conditions in engineered and natural systems vary widely (*1*, *2*, *26*−*28*), supporting our speculation of a lack of a "universality" of aggregate fractal dimensions in these systems.

Several investigators have examined aggregate settling by including a shape factor, ϕ, into Stokes' law, in the form

$$U = \frac{g\Delta\rho(1-p)}{\phi 18\nu\rho_l} d^2 \tag{30}$$

The reduction of drag observed here as a result of the fractal nature of the aggregate, however, is not the same phenomenon described by a shape factor. Settling velocities of nonspherical aggregates are decreased compared to those for spheres, not increased as observed in our studies.

The reduced drag coefficients calculated for the fractal microsphere aggregates may not be applicable to all types of aggregates since many aggregated particles, such as activated sludge flocs in engineered bioreactors and marine snow in the ocean, contain a variety of polymers, filaments and other material that can clog pores and alter the flow conditions around and within settling aggregates. Despite these possibilities, however, there is strong evidence for wide applicability of our observations. Marine snow (aggregates > 0.5 mm) exhibit fractal scaling properties for size−area and size−porosity relationships (*26*), and it is

thought that most marine snow is formed from smaller particles that also have fractal properties (*29*). Alldredge and Gottschalk (*30*) calculated that drag coefficients for marine snow were slightly higher than for impermeable spheres, but they used a relatively high particle density of 1.23 g cm^{-3} (typical of herbivore fecal pellets) in their calculations rather than lower densities more typical of bacteria, phytoplankton, or fecal pellets of planktonic predators such as chaetognaths (*31*). As shown above, lower particle densities would have reduced calculated drag coefficients. Drag coefficients reported for other marine particles, such as re-coagulated marine sediments, are much lower than expected for impermeable spheres even when an upper limit for the primary particle density of 2.65 g cm^{-3} is assumed (*8*, *9*).

Particle settling velocities are widely used in calculation of carbon fluxes to the sediments in the ocean as well as in many engineering calculations for water and wastewater treatment processes. While further work is necessary to strengthen the generality of our findings to other types of aggregates, our study suggests that previous calculations relating aggregate size and settling velocity based only on Stokes' law will need to be re-examined. The primary result will be that the mass fluxes estimated from settling velocity calculations will need to be changed to account for the faster settling velocities of fractal aggregates compared to impermeable spheres.

Acknowledgments

This research was supported by ONR Grant N00014-91-J-1249.

Literature Cited

(1) Li, D.-H.; Ganczarczyk, J. J. *Environ. Sci. Technol.* **1989**, *23*, 1385−1389.
(2) Logan, B. E.; Wilkinson, D. B. *Limnol. Oceanogr.* **1990**, *35*, 130−136.
(3) Han, M.; Lawler, D. F. *J. Am. Water Works Assoc.* **1992**, *84*, 79−91.
(4) Valiolis, I. A.; List, E. J. *Environ. Sci. Technol.* **1984**, *18*, 242−247.
(5) Yao, K. M.; Habibian, M. T.; O'Melia, C. R. *Environ. Sci. Technol.* **1971**, *5*, 1102−1112.
(6) Rajagopalan, R.; Tien, C. *Am. Inst. Chem. Eng. J.* **1976**, *22*, 523−533.
(7) Hawley, N. *J. Geophys. Res.* **1982**, *87*, 9489−9498.
(8) Kajihara, M. *J. Oceanogr. Soc. Jpn.* **1971**, *27*, 158−162.
(9) Gibbs, R. J. *J. Geophys. Res.* **1985**, *90*, 3249−3251.
(10) Bird, R. B.; Stewart, W. E.; Lightfoot, E. N. *Transport Phenomena*; Wiley: New York, 1960.
(11) Matsumoto, K.; Suganuma, A. *Chem. Eng. Sci.* **1977**, *32*, 445−447.
(12) Masliyah, J. H.; Polikar, M. *Can. J. Chem. Eng.* **1980**, *58*, 299−302.
(13) Adler, P. M. *J. Colloid Interface Sci.* **1981**, *81*, 531−535.
(14) Logan, B. E.; Hunt, J. R. *Limnol. Oceanogr.* **1987**, *32*, 1034−1048.
(15) Chellam, S.; Wiesner, M. R. *Water Res.* **1993**, *27*, 1493−1496.
(16) Tambo, N.; Watanabe, Y. *Water Res.* **1979**, 13, 409−419.
(17) White, F. M. *Viscous fluid flow*; McGraw Hill: New York, 1974; p 209.
(18) Meakin, P. *Adv. Colloid Interface Sci.* **1988**, *28*, 249−331.
(19) Jiang, Q.; Logan, B. E. *Environ. Sci. Technol.* **1991**, *25*, 2031−2037.
(20) Stolzenback, K. *Deep-Sea Res.* **1993**, *40*, 359−369.
(21) Lai, R. J.; Hudson, H. E., Jr.; Singley, J. E. *J. Am. Water Works Assoc.* **1975**, *67*, 553.
(22) Happel, J. *Low Reynolds Number Hydrodynamics, with special applications to particulate media*; Prentice Hall: Englewood Cliffs, NJ, 1965; p 385.
(23) Johnson, C. P. Settling velocities of fractal aggregates. M.S. Thesis, University of Arizona, 1995, 118 pp.
(24) Wiltzius, P. *Phys. Rev. Lett.* **1987**, *58*, 710−713.
(25) Rojak, S. N.; Flagan, R. C. *J. Colloid Interface Sci.* **1990**, *134*, 206−218.
(26) Kilps, J. R.; Logan, B. E.; Alldredge, A. L. *Deep-Sea Res.* **1994**, *41*, 1159−1169
(27) Namar, J.; Ganczarczyk, J. J. *Water Res.* **1994**, *27*, 1285−1294.
(28) Logan, B. E.; Kilps, J. R. *Water Res.* **1995**, *29*, 443−453.
(29) Li, X.; Logan, B. E. *Deep-Sea Res.* **1995**, *42*, 125−138.
(30) Alldredge, A. L.; Gottschalk, C. *Limnol. Oceanogr.* **1988**, *33*, 339−351.
(31) Dilling, L.; Alldredge, A. L. *Mar. Ecol. Prog. Ser.* **1993**, *92*, 51−58.

Received for review August 14, 1995. Revised manuscript received February 5, 1996. Accepted February 7, 1996.[⊗]

ES950604G

[⊗] Abstract published in *Advance ACS Abstracts,* April 1, 1996.